Static and Dynamic Anomalies in a Repulsive Spherical Ramp Liquid: Theory and Simulation

Pradeep Kumar[1], Sergey V. Buldyrev[1,2], Francesco Sciortino[3], Emanuela Zaccarelli[3], H. Eugene Stanley[1]

[1] *Center for Polymer Studies and Department of Physics*

Boston University,

Boston, MA 02215 USA

[2] *Yeshiva University,*

Department of Physics,

500 W 185th Street

New York, NY 10033 USA

[3] *Dipartimento di Fisica and INFM CRS-SOFT:*

Complex Dynamics in Structured Systems,

Università di Roma La Sapienza,

Piazzale Aldo Moro 5,

I-00185 Rome, Italy

(Dated: kbszs.tex 3 November 2004)

Abstract

We compare theoretical and simulation results for static and dynamic properties for a model of particles interacting via a spherically symmetric repulsive ramp potential. The model displays anomalies similar to those found in liquid water, namely, expansion upon cooling and an increase of diffusivity upon compression. In particular, we calculate the phase diagram from the simulation and successfully compare it with the phase diagram obtained using the Rogers-Young (RY) closure for the Ornstein-Zernike equation. Both the theoretical and the numerical calculations confirm the presence of a line of isobaric density maxima, and lines of compressibility minima and maxima. Indirect evidence of a liquid-liquid critical point is found. Dynamic properties also show anomalies. Along constant temperature paths, as the density increases, the dynamics alternates several times between slowing down and speeding up, and we associate this behavior with the progressive structuring and de-structuring of the liquid. Finally we confirm that mode coupling theory successfully predicts the non-monotonic behavior of dynamics and the presence of multiple glass phases, providing strong evidence that structure (the only input of mode coupling theory) controls dynamics.

I. INTRODUCTION

Water and some other liquids exhibit anomalous behavior close to their freezing lines [1, 2]. Their phase diagrams have regions characterized by a negative thermal expansion coefficient, i.e., these liquids expand upon cooling at certain temperatures and pressures. Besides the density anomaly, such liquids also have other peculiar thermodynamic and dynamic behaviors [3]. For example, the isothermal compressibility increases upon cooling and the diffusivity increases upon pressurizing. Usually the region of the diffusion anomaly is wider than the region of the density anomaly, so that the latter is completely contained in the former [4]. The anomalous behavior of the thermodynamic properties of water has been connected to the existence of a hypothetical liquid-liquid critical point in deeply supercooled states [5, 6, 7, 8]. In the case of water, this critical point is located in an experimentally unaccessible region. Recently, using the potential energy landscape formalism, it has been argued [5] that under certain assumptions on the statistical properties of the potential energy landscape, the existence of a density anomaly must lead to the existence of a liquid-liquid critical point.

In the case of water, anomalies are thought to be related to the tetrahedrality of the interparticle potential. On average, each water molecule has four nearest neighbors connected by hydrogen bonds. However, tetrahedrality is not a necessary condition for anomalous behavior and several spherically symmetric potentials that are indeed able to generate density and/or diffusion anomalies have been proposed [9, 10, 11, 12, 13, 14, 15, 16]. Interestingly, such potentials may be purely repulsive, providing evidence that different microscopic mechanisms can generate density anomalies. These potentials can be regarded as the simplest models which yield water-type thermodynamic and dynamic anomalies and it is important to fully characterize their thermodynamic and dynamic behavior. An additional advantage in studying spherical potentials is that their behavior can also be studied within a theoretical framework, for their thermodynamic properties can be calculated using accurate integral equation closures.

Here we study, using extensive molecular dynamics (MD) simulations, a specific, spherically symmetric repulsive potential introduced by Jagla [10, 11, 12, 13, 14] with the aim of fully characterizing both static and dynamic extreme loci in the temperature-density plane. We complement the MD study with integral theory calculations based on the (thermody-

namically consistent) Rogers-Young (RY) closure, which is known to give accurate results for other repulsive potentials, such as the square shoulder potential [17] and the star polymer potential [18, 19, 20]. We also compare numerical results in the low T region with predictions based on the ideal mode-coupling theory (MCT) [21, 22], which we solve using the RY static structure factors as input. We find that MCT is able to predict the non-monotonic behavior of dynamics and the presence of multiple glass phases, providing further evidence that structure (the only input of MCT) controls dynamics in this system.

II. METHODS

A. Discrete Molecular Dynamic Simulations

We study the linear ramp potential introduced by Jagla [10, 11, 12, 13, 14]

$$U(r) = \begin{cases} \infty & r < \sigma_0 \\ U_0(\sigma_1 - r)/(\sigma_1 - \sigma_0) & \sigma_0 < r < \sigma_1, \\ 0 & r > \sigma_1 \end{cases} \tag{1}$$

focusing on the specific choice of $\lambda \equiv \sigma_1/\sigma_0 = 1.76$, which has been studied previously by Jagla [10]. Using Monte Carlo simulations, Jagla showed that a density maximum is found in the liquid phase. For this choice of λ, the potential in Eq. (1) is a good candidate for studying the connection between thermodynamic and dynamic quantities. In order to study the dynamic properties, we apply the discrete MD method, approximating the continuous potential by a sequence of step functions with n small vertical steps,

$$U_n(r) = \begin{cases} \infty & r < \sigma_0 \\ k\Delta U & \sigma_1 - (k+\frac{1}{2})\Delta r < r < \sigma_1 - (k-\frac{1}{2})\Delta r \\ 0 & r > \sigma_1 - \frac{\Delta r}{2} \end{cases}, \tag{2}$$

where $\Delta r \equiv (\sigma_1 - \sigma_0)/(n + 1/2)$, $\Delta U \equiv U_0/(n + 1/2)$, and $k = 1, 2, 3, \ldots n$. The unit of length is σ_0, while U_0 is the unit of energy. Temperature is measured in units of energy, i.e., $k_B = 1$. Simulation time is measured in units of $\sigma_0\sqrt{m/U_0}$, with m as the particle mass, and pressure in units of U_0/σ_0^3. The number density is defined as $\rho \equiv N/L^3$, where L is the size of the simulation box and N is the number of particles.

The standard discrete molecular dynamics algorithm has been implemented for particles interacting with step potentials [23, 25, 26]. Between collisions, particles move along straight lines with constant velocities. When the distance between the particles becomes equal to the distance for which $U(r)$ has a discontinuity, the velocities of the interacting particles instantaneously change. The algorithm calculates the shortest collision time in the system and propagates the trajectories of particles from one collision to the next. Calculations of the next collision time are optimized by dividing the system into small sub-systems, so that collision times are computed only between particles in neighboring sub-systems. Since the total energy E is rigorously conserved, it is best to study the NVE-ensemble in the cubic box of a fixed volume $V = L^3$ with periodic boundary conditions.

We consider $N = 1728$ particles in our simulation. For constant temperature and pressure simulations, the Berendsen thermostat and barostat are used. Configurations in the NVE ensemble are saved on a logarithmic spacing for further processing, after discarding an initial equilibration period for a time larger than the correlation time at the particular state point [27]. The diffusion coefficient, measured in units of $\sigma_0\sqrt{U_0/m}$, is calculated as

$$D = \lim_{t\to\infty} \frac{\langle[\mathbf{r}(t'+t) - \mathbf{r}(t')]^2\rangle_{t'}}{6t}, \tag{3}$$

where $\langle\ldots\rangle_{t'}$ denotes an average over all particles and over all t'. The dynamic structure factor for a given vector $\mathbf{q}$ is defined as

$$S(\mathbf{q},t) \equiv \left\langle \frac{1}{N}\sum_{i,j}^{N} \exp(i\mathbf{q}\cdot[\mathbf{r}_i(t'+t) - \mathbf{r}_j(t')]) \right\rangle_{t'}, \tag{4}$$

where $\langle\ldots\rangle_{t'}$ denotes the average over all t' and $S(\mathbf{q}) \equiv S(\mathbf{q},0)$ is the static structure factor. The normalized structure factor

$$\phi(\mathbf{q},t) \equiv \frac{S(\mathbf{q},t)}{S(\mathbf{q},0)} \tag{5}$$

is called the density correlator. The isotropy of the liquid allows us to average $S(\mathbf{q},t)$ over different $\mathbf{q}$ with the same modulus. In the following, we bin together all $\mathbf{q}$ within a mesh $\Delta q = \pi/L$.

B. Rogers-Young Closure

Integral equation theories are powerful tools for studying the structure and thermodynamic properties of liquids [28, 29]. One assumes a two-body interaction potential for the

particles and introduces the total pair correlation function $h(r)$, related to the pair distribution function $g(r) \equiv h(r) + 1$, and the direct correlation function $c(r)$. The goal is to solve the self-consistent Ornstein-Zernike equation,

$$h(r) = c(r) + \rho \int dr' c(|\mathbf{r} - \mathbf{r}'|) h(r'), \tag{6}$$

where both $c(r)$ and $h(r)$—or, equivalently, $g(r)$—are unknown. Equation (6) in Fourier space takes the form

$$h(q) = c(q) + \rho c(q) h(q), \tag{7}$$

where $c(q)$ is related to $S(q)$ as $c(q) = (1 - 1/S(q))/\rho$.

According to the particular form of the interaction potential $U(r)$, one can choose a certain ansatz for $c(r)$, which relates it to the interaction potential and to $h(r)$ and allows one to solve Eq. (6) analytically in some cases [28] and numerically otherwise. The two frequently employed closures, Percus-Yevick (PY) or the hypernetted chain (HNC) [29], suffer from being thermodynamically inconsistent [28]. This means that although they can provide good estimates of the static structure factor, they cannot be reliably used for determining the phase diagram of the system. More sophisticated closures have thus been developed in recent years, which have a built-in thermodynamic consistency. This is achieved by introducing an extra parameter in the ansatz, which can then be determined to fulfill such a condition.

The RY closure [30] belongs to the thermodynamically consistent group of closures obtained by appropriately mixing PY and HNC through the parameter ζ. The ansatz for $c(r)$ in terms of $h(r)$ becomes

$$c(r) = \exp[-\beta U(r)] \left[1 + \frac{\exp[(h(r) - c(r)) f(r)] - 1}{f(r)} \right] - [h(r) - c(r) + 1], \tag{8}$$

where $f(r)$ is the 'mixing function',

$$f(r) \equiv 1 - \exp(-\zeta r). \tag{9}$$

For $\zeta = 0$, one recovers PY closure, while for $\zeta \to \infty$ Eq. (8) reduces to the HNC condition.

The OZ equation can be solved using Eq. (8) for a given value of ζ. The correct solution corresponds to that value of ζ for which the compressibilities K_T, calculated using the "virial" and the "fluctuations" routes agree, ensuring thermodynamic consistency. This allows us to reliably use the RY closure not only to calculate the static structure factor, but

also the phase diagram, as we will do in the following. Moreover, RY gives particularly good results for a purely repulsive potential, such as the studied ramp potential. It has already been successfully tested against simulations for square shoulder potentials [17], and for both experiments and simulations for the star polymer effective potential [18, 19, 20, 31].

C. Mode Coupling Theory

The density correlator defined in Eq. (5) is the fundamental quantity of interest in MCT, a set of generalized coupled Langevin equations which can be closed within certain approximations [21, 22]. Interesting behavior of these observables arise when the dynamics of the system becomes slower, i.e., when the dynamical behavior is of the "supercooled" type [32]. A typical two-step relaxation occurs for the density correlators on approaching dynamical arrest, indicating the emergence of two distinct time scales in the system's structural relaxation. A first relaxation process, the β relaxation, occurs at short times, and is due to particles exploring the cages formed by their nearest neighbors. A second relaxation, the α relaxation, occurs at longer time scales, when particles are able to escape the cages. MCT predicts the existence of a glass transition at a characteristic temperature T_{MCT}, where the time scale of this second relaxation τ_α diverges so that the particles will always remain trapped in their cages. For $T < T_{MCT}$ the correlators do not relax any more, reaching a finite plateau value at long t, defined as the nonergodicity parameter $f(q) \equiv \lim_{t\to\infty} \phi(q,t)$; $f(q)$ jumps discontinuously from zero to a finite (critical) value $f_c(q)$ at the transition, signaling the occurrence of an ergodic (fluid) to a nonergodic (glass) transition. The transition is kinetic, i.e., nothing happens at the thermodynamic properties of the system close to T_{MCT}.

MCT predictions are often found to be in agreement with experimental [33] and simulation results [34], although in real systems the α-relaxation time does not diverge, but only becomes increasingly larger. This is due to the intervention of other processes, commonly termed "hopping" processes, which restore ergodicity and are not included in the MCT treatment of the ideal glass transition described above.

In mathematical terms, the non-ergodicity parameters $f(q)$ are the long time solutions of the MCT equations, i.e.,

$$\frac{f(q)}{1-f(q)} = m(q), \tag{10}$$

where the memory kernel $m(q)$ is quadratic in the correlator

$$m(q) = \frac{1}{2}\int \frac{d^3k}{(2\pi)^3}\mathcal{V}(\mathbf{q},\mathbf{k})f(k)f(|\mathbf{q}-\mathbf{k}|), \tag{11}$$

where $k = |\mathbf{k}|$. The vertex functions $\mathcal{V}$ are the coupling constants of the theory, which are given only in terms of the static structure factor and number density of the system,

$$\mathcal{V}(\mathbf{q},\mathbf{k}) = \frac{\rho}{q^4}\left[\mathbf{q}\cdot(\mathbf{q}-\mathbf{k})\; c(|\mathbf{q}-\mathbf{k}|) + \mathbf{q}\cdot\mathbf{k}\; c(k)\right]^2 \times S(q)S(k)S(|\mathbf{q}-\mathbf{k}|). \tag{12}$$

Equations (10) and (11) define a system of non linear equations with a trivial solution $f(q) = 0$. However, for certain values of the vertex functions, the solutions have a bifurcation point, locating the glass transition. At this transition point a solution $f(q) > 0$ emerges. The time evolution of the density correlators is found by solving the full MCT equations,

$$\ddot{\phi}(q,t) + \Omega^2(q)\phi(q,t) + \int_0^t m(q,t-t')\dot{\phi}(q,t')\,dt' = 0\;, \tag{13}$$

where $\Omega^2(q) \equiv q^2/(\beta m S(q))$ and $m(q,t)$ is the time-dependent memory kernel

$$m(q,t) \equiv \frac{1}{2}\int \frac{d^3k}{(2\pi)^3}\mathcal{V}(\mathbf{q},\mathbf{k})\phi(k,t)\phi(|\mathbf{q}-\mathbf{k}|,t). \tag{14}$$

The two-step relaxation is well described by MCT through an asymptotic study of the correlators near the ideal glass solutions. The α-relaxation is effectively described by a stretched exponential,

$$\phi(q,t) = A_q \exp[-(t/\tau_q)^{\beta_q}], \tag{15}$$

where the amplitude A_q determines the plateau value and $\beta_q < 1$.

MCT predicts a power-law divergence of the α-relaxation time as well as a power-law decrease of the diffusivity as the system approaches the ideal glass transition. In this study, we compare the dynamic behavior evaluated from the MD simulations with corresponding MCT predictions.

III. RESULTS

A. Dependence on the Number of Steps in the Ramp

We first study how the results of molecular dynamic simulations for the potential $U_n(r)$ in Eq. (2) converge to the results for the continuous ramp potential $U(r)$ in (1), as $n \to \infty$

where n is the number of approximating steps. The exact equation of state for systems described by a pair potential can be calculated from the partition function, i.e., by the integral $\int\int ... \int \exp[-\sum_{i>j} U(\mathbf{r}_i - \mathbf{r}_j)/k_BT] \prod_{i=1}^{N} d\mathbf{r_i}$. Replacing the continuous potential $U(\mathbf{r}_i - \mathbf{r}_j)$ by a step-function is analogous to replacing an integral by a sum in a rectangular approximation which is known to converge to the integral as $1/n^2$. Thus we can expect that the pressure P_n obtained in the discrete molecular dynamics for given n converges to the value for the continuous potential P_∞ as $1/n^2$. On the other hand, the probability for a particle to jump over a step of size ΔU is proportional to $\exp(-\Delta U/k_BT) \sim 1 - U_0/nk_BT$. The diffusion coefficient must be a differentiable function of this probability. Thus we can expect that the diffusion constant D_n in discrete MD approaches its limiting value D_∞ as $1/n$. Figures 2(a) and 2(b) confirm these predictions. In the following, we limit ourselves to the case $n = 144$ which, as shown in Figs. 2(a) and 2(b), is sufficiently close to the $n \to \infty$ case.

B. Structure Factors and Comparison with RY

Figure 3 shows the density dependence of the structure factor, as calculated from the MD at $T = 0.063$. At this low T the liquid, even at low densities, is significantly structured, as shown by the large amplitude of the first peak. On increasing the density, contrary to the normal liquid behavior, the amplitude of the first peak is reduced. As discussed below, the destructuring of the liquid is associated to a speed-up of the particle dynamics. If ρ is further increased, the second peak becomes dominant and (as discussed in the following) its increase correlates with a slowing down of the dynamics. The first peak is significantly reduced and acts as a pre-peak on the major peak. The crossover of the leading amplitude from the first to the second peak resembles the behavior previously discovered in star-polymers of large functionality [35]. In these systems, the star-star interaction can be effectively reduced to an ultra-soft repulsive logarithmic interaction [18]. However, the peak positions of $S(q)$ change positions with density in this case, as opposed to what is found in ramp potential.

Figures 4(a)–4(d) compare the static structure factor calculated using simulation data along with the results of the RY-closure for several densities at $T = 0.063$. A tolerance of 5.10^{-5} is used for the thermodynamic consistency. The RY integral theory provides a correct description of the ρ dependence of the dynamics. RY correctly predicts the structure factor

at high densities, while for intermediate and low densities RY gives a fairly good estimate of the structure factor except that the first peak in the structure factor is lower than the one calculated from simulation. RY thus tends to underestimate the structure of the liquid.

C. Phase Diagram

Figure 5 shows the phase diagram of the model obtained by slow cooling (thin lines representing isochores) and by accurate simulations of individual state points (circles). The simulations for each density and temperature are initialized with random configurations and are equilibrated to the desired temperature using Berendsen's thermostat for a sufficient period of time. The equilibration time was estimated as the time when the density correlator $\phi(\mathbf{q}, t)$ at the first peak of $S(q)$ decays to zero. After equilibration, each configuration was left to run at constant energy for a time dependent on the speed of the dynamics, covering at least ten equilibration times. The temperature of maximal density (TMD), shown by a bold line, was obtained by connecting the points on each isochore corresponding to the minimal pressure, since these points correspond to the points of minimal volume due to the general relation

$$\left(\frac{\partial V}{\partial T}\right)_P = -\left(\frac{\partial P}{\partial T}\right)_V \left(\frac{\partial V}{\partial P}\right)_T \tag{16}$$

and $(\partial V/\partial P)_T < 0$ for a mechanically stable system. Thus, volume increases upon cooling at constant pressure in the region to the left of the TMD line.

At low T, the system spontaneously crystallizes during the time of the simulation in different crystalline forms. Consistent with Jagla's calculation ([10]), we find that:

(i) At low densities, the system crystallizes into a face centered cubic crystal structure upon slow cooling, when the temperature reaches the values indicated by crosses. The crystallization is marked by a sharp drop in the potential energy, associated with a fast release of latent heat. The line connecting these points can be regarded as a line of homogeneous nucleation. It has a marked negative slope, corresponding to the smaller density of the crystalline phase compared to liquid. The equilibrium melting line, which also has negative slope, is located at much higher temperatures, so that a large portion of the density anomaly lies in the supercooled state. This situation is completely analogous to the situation in water, in which the region of the density

anomaly is located near the negatively-sloped freezing line. In the ramp model, the anomaly does not exist below $\rho = 0.2432$, where the line of the *minimal* density merges with the line of the *maximal* density. Interestingly, the slope of the homogeneous nucleation line becomes positive below this density, as in a normal liquid where the crystal phase has a larger density than in the liquid phase. This behavior may exist in stretched water at negative pressures but has never been observed experimentally or in simulations.

(ii) In the region of intermediate densities $0.317 < \rho < 0.352$ the liquid does not crystallize and enters the glassy state below $T < 0.042$. We are not able to equilibrate the system below this temperature.

(iii) For $\rho > 0.352$, the system crystallizes into a rhombohedral crystal after being equilibrated for a long time at $T = 0.041$. Interestingly, the density anomaly vanishes at densities slightly lower than the density at which this new crystal phase emerges. This crystalline phase is characterized by parallel columns formed by equidistantly spaced atoms. The spacing among these atoms is slightly larger than the hard core distance. Thus in this crystalline phase each atom has two neighbors in its repulsive ramp. The projection of these columns onto a perpendicular plane forms a triangular lattice with spacing approximately equal to the diameter of the repulsive ramp. The columns are shifted with respect to each other by one third of the nearest-neighbor spacing so that the atoms form three crystalline planes, perpendicular to the columns. In each of these planes atoms form a triangular lattice with a spacing $\sqrt{3}$ times larger than the spacing in the triangular lattice formed by the projection of the columns.

(iv) A third distinct (hexagonal) crystalline phase is observed for $\rho \approx 0.7865$ (outside the range of densities explored in Fig. 5). At this state point the liquid, after some initial equilibration, crystallizes into a crystalline phase characterized by a hexagonal symmetry of one of its crystalline planes. This crystalline type is also formed by parallel columns consisting of equidistantly spaced atoms. The spacing among these atoms is slightly larger than the hard core distance. The projection of these columns onto a perpendicular plane forms a hexagonal lattice with spacing slightly smaller than the hard core. This spacing is equal to $\sqrt{3}/2$ of the distance between atoms in the columns. The neighboring columns are shifted with respect to each other by one half

of the atom spacing in the columns, so that the atom and its two neighbors in the neighboring column form an equilateral triangle. Thus in this crystalline type, each atom has eight nearest neighbors in its repulsive ramp: two in the same column and six in the three neighboring columns.

(v) For even larger densities not studied in this work, hexagonal close packed and finally hard-sphere face cubic centered crystals are expected [10].

We now discuss the possibility of a liquid-liquid critical point in this model. By quadratically extrapolating the isochores into the glassy state, we observe a crossing at very low temperatures. This crossing of the near density isochores is equivalent to $\partial P/\partial V|_T = 0$ and hence predicts the existence of a critical point with coordinates $T \approx 0.025$, $P \approx 0.838$, and $\rho \approx 0.346$, close to the largest density at which an isochore develops a negative slope. Interestingly, the TMD line, if extrapolated, appears to go directly to this putative critical point.

Another characteristic feature is the behavior of the isothermal compressibility, which shows an anomalous increase upon cooling between the lines of maximal and minimal compressibility, are shown in red in Fig. 5(a). The part of the low density branch with a positive slope corresponds to a compressibility minima, while the high density branch corresponds to the compressibility maxima. As in water and other materials, the isothermal compressibility line crosses the TMD line at the point of its maximal temperature (vertical slope) due to the mathematical properties of the second derivative of the equation of state [36]. Again, as in water, the line of compressibility maxima, if extrapolated, seems to approach the putative critical point.

Since the RY closure is thermodynamically consistent, it is possible to evaluate the phase diagram theoretically as well. Indeed, once the static structure factor $S(k)$ is obtained, the pair correlation function $g(r)$ can be calculated by taking the inverse Fourier transform of $S(k)$. All other thermodynamic quantities are calculated using the inter-particle potential function $U(r)$ and $g(r)$. In Fig. 5(b) we show the phase-diagram consisting of eight isochores of the system calculated using RY. Comparing Fig. 5(a) and Fig. 5(b), we can see that the RY predicts a smaller value of the pressure and also that the density maxima points are shifted to higher volumes. Despite this discrepancy in P, the shape of the isochores is very well reproduced. Even in the RY case, density maxima line appears in the phase diagram.

While in the simulation, extremely slow dynamics prevents access to the region where the critical point is probably located, in the RY calculations, no convergence of the parameter ζ is achieved in the same region. Again, a smooth extrapolation of the calculated isochores is consistent with a crossing point, and hence a critical point.

The thermodynamic behavior discussed above is analogous to the behavior of the one-dimensional model for which an exact solution can be obtained (see Appendix).

D. Dynamics

Next we focus on the dynamic properties of the model. Figure 5(a) shows the lines of diffusivity maxima and minima, i.e., the locus of points where $\partial D/\partial P|_T = 0$ in the phase diagram. The region of the anomalous increase of D upon compression ($\partial D/\partial P|_T > 0$) embraces the region of density anomaly as it does in two-dimensional models as well as in water [4, 23].

Figure 6(a) shows the density dependence of D along several isotherms in a density range extending to $\rho = 0.7$. While only one minimum and one maximum are observed at high T, at low T, data suggest the possibility of a more complex behavior of the density dependence of D. Indeed, for the range of densities $0.492 < \rho < 0.579$, the diffusion coefficient drops sharply for $T < 0.067$, and then recovers at higher densities, suggesting the presence of more than one locus of diffusion maxima. It is interesting to observe that this second maximum separates regions with different underlying crystal structures (orthorhombic and hexagonal) [37], similar to the location of the low ρ maximum, separating regions where the fcc and orthorhombic crystals are respectively stable.

It is interesting to compare the ρ dependence of the characteristic times numerically calculated with the prediction of mode coupling theory using RY results for $S(q)$ (MCT-RY). A comparison with the dynamics predicted by MCT can be performed by comparing the T and ρ dependence of D with the T and ρ dependence of the (inverse) characteristic time scale of decay of density fluctuations. This time can be calculated within MCT, from the solutions of Eq. (13). More specifically, for each wavevector q, the decay time can be defined as the value at which $\phi(q,t)$ reaches the value $1/e$. Figure 6(b) shows the inverse relaxation time at the wavevector corresponding to the first peak of the structure factor τ_1^{-1} as a function of ρ for different T. The same sequence of minima and maxima characteristic

of the MD diffusivity data is also found in the prediction of MCT-RY. This agreement is consistent with the possibility that the structure factor, the only input in the MCT, also encodes the system's dynamic properties.

To better characterize the low temperature dynamics and investigate the possibility of different glasses, we next study the decay of the density autocorrelation functions $\phi(q,t)$ as a function of t at $T = 0.063$ in Fig. 7, and calculate $\phi(q,t)$ from the MD trajectories Fig. 7(a). The non-monotonic behavior of D and τ_1 discussed in the previous figure is also seen in the decay of $\phi(q,t)$. At the highest studied density $\rho > 0.787$, the correlator does not decay to zero in the time scale of our simulations. For lower ϕ, the decay becomes faster until $\phi = 0.352$ and then it starts to slow down again. For $\phi < 0.26$, crystallization prevents the approach to a glass state. The decay of the correlation functions (at q corresponding to the first peak of the structure factor) can be well represented via a stretched exponential decay [Eq. (15)] at very high densities, $\rho = 0.702$ ($\beta = 0.89$), and by simple exponential decay ($\beta = 1$) at low ρ. A similar behavior is seen in Fig. 7(b) where the predictions of the MCT equations are shown. Again, on decreasing ρ, first a speed-up and then a slowing down of the dynamics is observed.

To quantify the comparison between MD and MCT-RY, we show the density dependence of τ_1 and τ_2 in Fig. 8 (the characteristic time of the first and second peaks of the structure factor respectively) both from MD and MCT-RY. The two sets of data show the same anomalous behavior, showing the minimum corresponding to the maximal diffusivity at the same ρ.

It is interesting to observe that while the slowing down of dynamics can be numerically followed for a large dynamical range at a high density, a low density crystallization prevents the generation of a glass structure. Unlike in MD, RY solutions can be found in a wider density range. It is thus interesting to ask whether a glass line is predicted by MCT-RY at low densities and, if so, how the two glasses differ. By solving the MCT equations for a wider range of densities, we find two distinct glasses at $T = 0.052$: $\rho = 0.682$ and $\rho = 0.257$. These two glasses are characterized by different critical non-ergodicity parameters (shown in Fig. 9). While the low density glass non ergodicity factor is similar to the one found in hard sphere systems, the high density glass is characterized by large amplitudes both at the first and second peak of $S(q)$. This resembles the one found in star polymers at high density, though the amplitude of the second peak in the latter becomes larger than that of the first

peak.

IV. SUMMARY AND CONCLUSIONS

In this work we have presented a systematic numerical study of the static and dynamic properties of a system of particles interacting with a spherical repulsive potential, with a range of interaction of the order of the particle diameter. The simplicity of the model makes it possible to study it with efficient numerical algorithms and, theoretically, with self-consistent integral theories [28]. Our results accomplish the following:

(i) They confirm the previous theoretical calculations by Jagla [10] concerning the existence of a line of density maxima in the phase diagram of this potential. Results also provide an accurate evaluation of this line as well as of the line of compressibility maxima and minima.

(ii) They confirm that different crystal structures are found at low temperatures, depending on the density [10], and provide estimates of the homogeneous nucleation line for the liquid-crystal transitions.

(iii) They provide evidence of the possibility of a liquid-liquid critical point at $T \approx 0.025$, $P \approx 0.838$ and $\rho \approx 0.346$. The location of the critical point is below the homogeneous nucleation line or glass transition line and cannot be accessed by simulations. A theoretical RY calculation of the phase diagram is able to reproduce the thermodynamic anomalies. These calculations also suggest the possibility of a liquid-liquid critical point but, again, its precise location cannot be determined due to the impossibility of equating the "virial" and "fluctuation" compressibilities with enough accuracy in this region of the phase diagram. Thus the existence of the critical point proposed by the extrapolation of the equation of state into the deeply supercooled region remains questionable [38].

(iv) They show that the RY closure agrees reasonably well with simulations of the system with the repulsive ramp potential and that it reproduces the static and dynamic anomalies. The RY closure slightly underestimates the pressure, and shifts the anomalies to a region of lower density.

(v) They provide evidence that dynamic anomalies in this model have a structural origin and they are indeed captured by the MCT-RY theory, which uses only structural information as input. Diffusion anomalies are encountered before the density anomalies, consistent with the case of water [4].

(vi) They suggest the possibility of different types of glasses in this simple system, consistent with the existence of different crystalline phases. A more extensive study based on the MCT-RY may help evaluate the location and the intersections [39, 40, 41] between different glass transition lines.

Acknowledgments

We thank C. Likos for help with the RY-closure and for extensive discussions. We also thank NSF Chemistry Grants No. CHE0096892 and No. CHE0404673 and MIUR Cofin 2001 and Firb 2002, and MRTN-CT-2003-504712 for support.

APPENDIX A: ONE DIMENSIONAL SYSTEM

Applying the Takahashi method [42], one can find the equation of state for the one-dimensional system of particles interacting via the ramp potential [see Eq. (1)]. In this case, the partition function Ψ for the Gibbs potential $G(P,T)$ can be factored, so that

$$G = -\frac{1}{\beta} N \ln \Psi(P,T), \tag{A1}$$

where

$$\Psi(P,T) = \int_0^\infty \exp\left(-\beta\left(U(r) + Pr\right)\right) dr. \tag{A2}$$

Substituting Eq. (1) into Eq. (A2) and integrating, we find that

$$\Psi(P,T) = \frac{\exp[-\beta(P\sigma_0 + U_0)] - \exp(-\beta P\sigma_1)}{\beta(P - P_c)} + \frac{\exp(-\beta\ P\sigma_1)}{\beta P}, \tag{A3}$$

where $\beta \equiv 1/k_B T$ and $P_c = U_0/(\sigma_1 - \sigma_0)$. Since $V \equiv (\partial G/\partial P)_T$

$$\rho \equiv N/V = -\frac{\beta\Psi}{(\partial\Psi/\partial P)_T}, \tag{A4}$$

which, after differentiation, leads to

$$\rho = \frac{\frac{e^{-\beta(U_0+\sigma_0 P)}}{(P-P_c)} + e^{-\beta\sigma_1 P}[\frac{1}{P} - \frac{1}{(P-P_c)}]}{e^{-\beta(U_0+\sigma_0 P)}[\frac{\sigma_0}{(P-P_c)} + \frac{1}{\beta(P-P_c)^2}] + e^{-\beta\sigma_1 P}[\frac{\sigma_1}{P} - \frac{\sigma_1}{(P-P_c)} + \frac{1}{\beta P^2} - \frac{1}{\beta(P-P_c)^2}]} \tag{A5}$$

Note that P_c plays the role of a critical pressure, at which the equation of state becomes discontinuous for $T \to 0$. Indeed,

$$\lim_{T\to 0} \rho = \begin{cases} 1/\sigma_0 & P > P_c \\ 2/(\sigma_1 + \sigma_0) & P = P_c \\ 1/\sigma_1 & P < P_c \end{cases} . \tag{A6}$$

Hence, an infinitesimal increase of pressure around P_c and small T leads to a finite increase of density from $1/\sigma_1$ for $P < P_c$ to $1/\sigma_0$ for $P > P_c$. Thus, in the one-dimensional system, there is an analog of a critical point at $T = T_c = 0$, $P = P_c$, and $\rho = \rho_c$, at which the isothermal compressibility diverges. At $P = P_c$, Eq. (A5) simplifies to

$$\rho = \frac{1 + k_B T/U_0}{(\sigma_0 + \sigma_1)/2 + (k_B T/U_0)\sigma_1 + (k_B T/U_0)^2(\sigma_1 - \sigma_0)}. \tag{A7}$$

For $P < P_c$ there exists a region in which there is a density anomaly and a region in which there is a compressibility anomaly, exactly as in the three-dimensional model studied in this work.

The isochores described by Eq. (A5) are plotted in Fig. 10. One can see that the temperature of maximal density approaches the critical point as $P \to P_c$.

---

[1] P. Debenedetti, J. Phys.: Condens. Matter **15**, R1669 (2003).

[2] C. A. Angell, Ann. Rev. Chem. **55**, 559 (2004).

[3] P. G. Debenedetti, *Metastable Liquids: Concepts and Principles* (Princeton University Press, Princeton, 1998).

[4] J. R. Errington and P. G. Debenedetti, Nature **409** 318 (2001).

[5] F. Sciortino, E. La Nave, and P. Tartaglia, Phys. Rev. Lett. **91**, 155701 (2003).

[6] P. H. Poole et al., Nature (London) **360**, 324 (1992); F. Sciortino et al., Phys. Rev. E **55**, 727 (1997); S. T. Harrington et al., J. Chem. Phys. **107**, 7443 (1997); M. Yamada et al., Phys. Rev. Lett. **88**, 195701 (2202).

[7] P. H. Poole et al., Phys. Rev. Lett. **73**, 1632 (1994).

[8] O. Mishima and H. E. Stanley, Nature **392**, 164 (1998).

[9] F. H. Stillinger and D. K. Stillinger, Physica A **244**, 358 (1997).

[10] E. A. Jagla, J. Chem. Phys. **111**, 8980 (1999); Phys. Rev. E **63**, 061509 (2001).

[11] M. R. Sadr-Lahijany et al., Phys. Rev. Lett. **81**, 4895-4898 (1998); Phys. Rev. E **60**, 6714–6721 (1999).

[12] A. Scala et al., J. Stat. Phys. **100** 97–106 (2000); Phys. Rev. E **63** 041202 (2001).

[13] S. V. Buldyrev et al., in *New Kinds of Phase Transitions: Transformations in Disordered Substances*, NATO Advanced Research Workshop, Volga River, edited by V. Brazhkin et al., (Kluwer, Dordrecht, 2002), pp. 97–120.

[14] P. C. Hemmer and G. Stell, Phys. Rev. Lett. **24**, 1284 (1970); G. Stell and P. C. Hemmer, J. Chem. Phys. **56**, 4274 (1972); J. M. Kincaid and G. Stell, J. Chem. Phys. **67**, 420 (1977); J. M. Kincaid, G. Stell and E. Goldmark, J. Chem. Phys. **65**, 2172 (1976); J. M. Kincaid, G. Stell and C. K. Hall, J. Chem. Phys. **65**, 2161 (1976).

[15] F. H. Stillinger, Chem. Phys. **65**, 3968 (1976).

[16] G. Franzese et al., Nature **409**, 692 (2001).

[17] A. Lang et al., J. Phys.: Cond. Mat. **11**, 10143 (1999).

[18] C. N. Likos et al., Phys. Rev. Lett. **80**, 4450 (1998).

[19] M. Watzlawek, C. N. Likos, and H. Löwen Phys. Rev. Lett. **82**, 5289 (1999).

[20] M. Laurati et al., submitted (2004).

[21] U. Bengtzelius, W. Götze, and A. Sjölander, J. Phys. C: Solid State Phys. **17**, 5915 (1984).

[22] W. Götze, *Liquids, Freezing, and Glass Transition*, edited by J. P. Hansen, D. Levesque, and J. Zinn-Justin (North-Holland, Amsterdam, 1991), p. 287.

[23] S. V. Buldyrev et al., Physica A **304**, 23–42 (2002).

[24] S. V. Buldyrev and H. E. Stanley, Physica A **330**, 124 (2003)

[25] A. Skibinsky et al., Phys. Rev. E **69**, 061206 (2004).

[26] D. C. Rapaport, *The Art of Molecular Dynamic Simulation* (Cambridge University Press, Cambridge, 1995).

[27] Configurations are saved at times $t_{jk} \equiv (js^m + s^k)\Delta t$, where $k = 0, 1, ..., m$ and $j = 0, 1, ..., j_{\max}$, For the majority of our state points we use $\Delta t = 0.03082207$, $m = 14$, $j_{\max} = 100$ and $s = 2$.

[28] C. Caccamo, Physics Reports **274**, 1 (1996).

[29] J. P. Hansen and I. R. McDonald, *Theory of Simple Liquids* (Academic, London, 1976).

[30] F. A. Rogers and D. A. Young, Phys. Rev. A **30**, 999 (1984).

[31] C. Mayer, C. N. Likos, and H. Loewen, Phys. Rev. E **70**, 041402 (2004).

[32] For the case of slow dynamics in water see for example F. Sciortino et al., Phys. Rev. E **54** 6331 (1996); F. Sciortino et al., Phys. Rev. E **56** 5397 (1997); L. Fabbian et al., J. Non-Cryst. Solids **235-237**, 350 (1998); F. Starr et al., Phys. Rev. E **60** 6757 (1999).

[33] For a recent review on the comparison between experimental data and MCT predictions see: W. Götze, J. Phys.: Condens. Matter **11**, A1 (1999).

[34] M. Nauroth and W. Kob, Phys. Rev. E **55**, 675 (1997); C. Theis et al., Phys. Rev. E. **62**, 1856 (2000); F. Sciortino and W . Kob, Phys. Rev. Lett. **86**, 648–651 (2001);

[35] M. Watzlawek, C. N. Likos and H. Loewen, J. Phys.: Condens. Matter **10**, 8189 (1998).

[36] S. Sastry et al., Phys. Rev. E **53** 6144 (1996)

[37] One may expect that this part of the phase diagram corresponds to partial crystallization. However, the behavior of the system in this region of the phase diagram does not resemble crystallization, which at other regions of the phase diagram is characterized by a sharp decrease of potential energy with a latent heat release. The potential energy at these state points slowly decreases with time, resembling the aging of glasses. Also, upon heating to a slightly larger temperature, $T = 0.0684$ (for which no anomalous behavior of diffusion coefficient is observed), the system slowly relaxes back to the normal liquid phase. In contrast, spontaneous crystallization usually happens in a deeply supercooled state so that the true crystal does not melt if the temperature is slightly increased. Also, the structure factors of these phases do not develop large, high q peaks, characteristic of the crystalline phase. Thus the nature of these intermediate phases is not clear.

[38] E. A. Jagla, Braz. J. Phys. **34**, 17 (2004).

[39] L. Fabbian et al., Phys. Rev. E **59**, R1347 (1999); Phys. Rev. E **60**, 2430 (1999); F. Sciortino, Nature Mater. **1**, 45 (2002).

[40] E. Zaccarelli et al., Phys. Rev. E **66**, 041402 (2002).

[41] K. Dawson et al., Phys. Rev. E **63** 011401 (2001).

[42] E. H. Lieb and D. C. Mattis, *Mathematical Physics in One Dimension* (Academic, New York, 1966), p. 2.

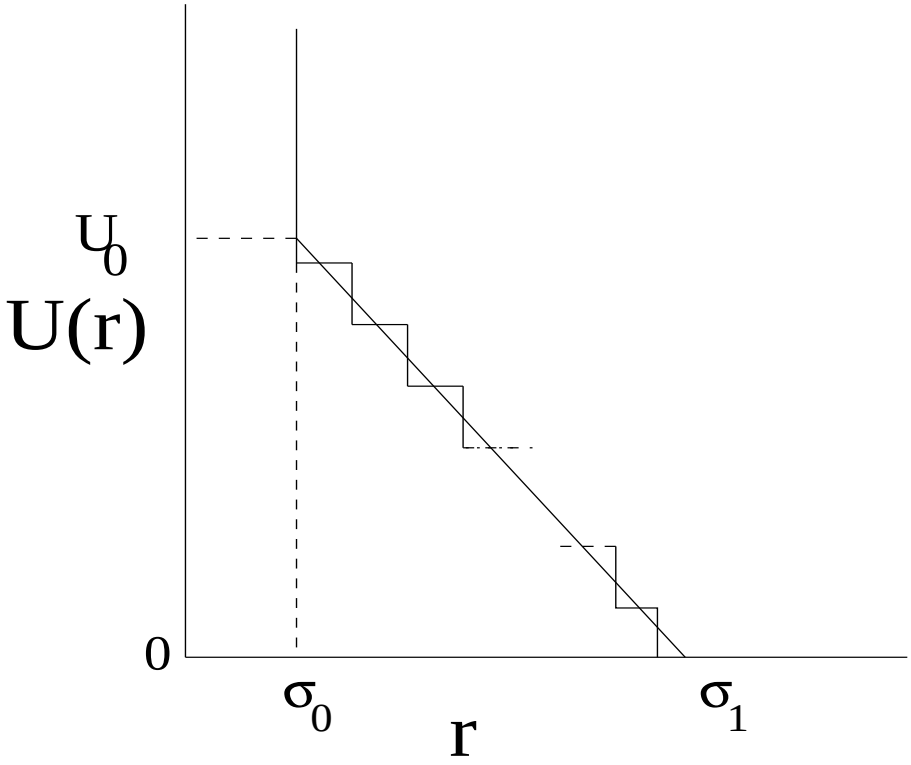

FIG. 1: Schematic representation of the repulsive ramp potential (1) and its discontinuous version (2).

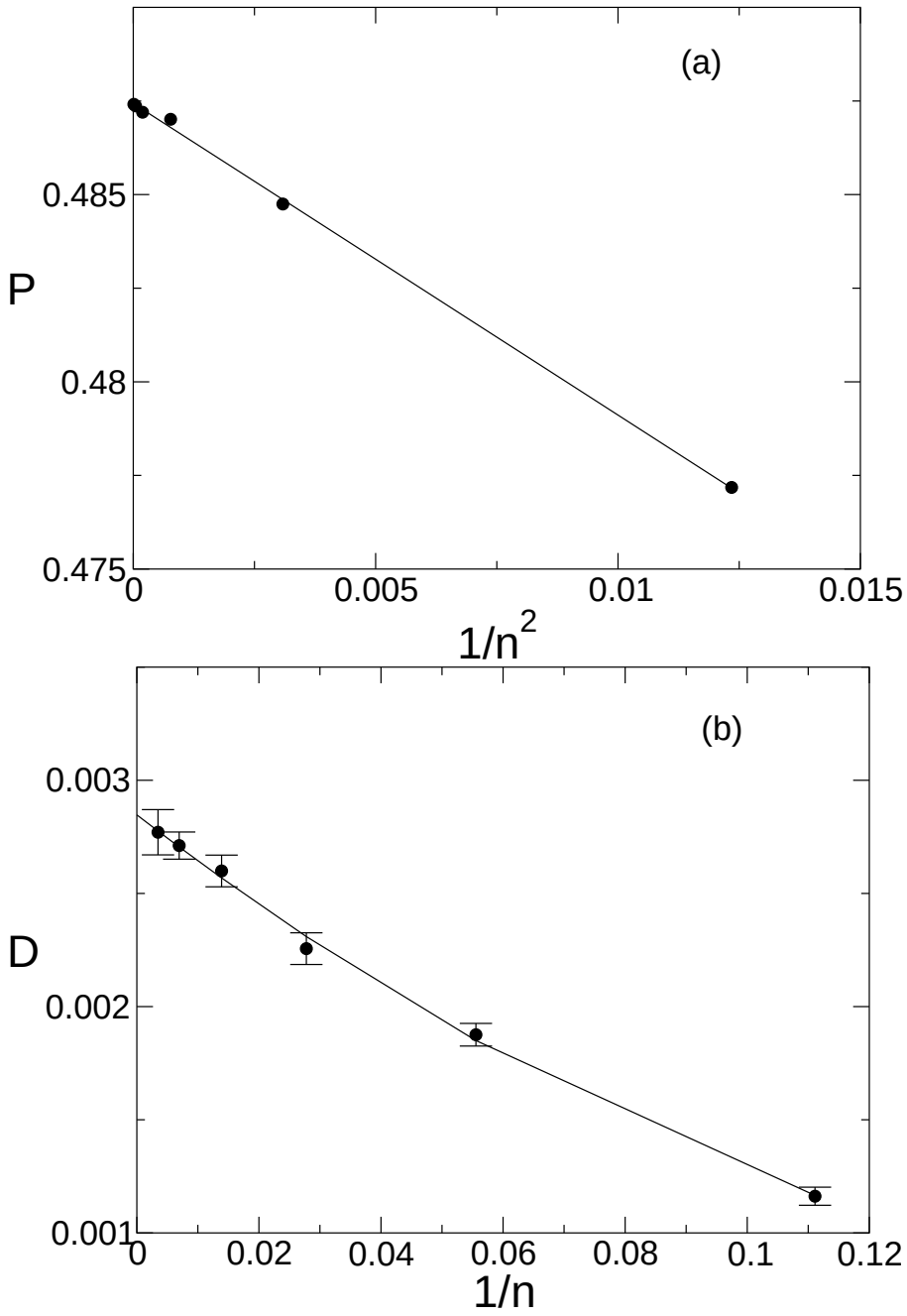

FIG. 2: (a) Pressure P as a function of n^{-2} [where n is defined in Eq. (2)] for $T = 0.063$ and $\rho = 0.260$. (b) Diffusion coefficient D as a function of n^{-1} for the same state point.

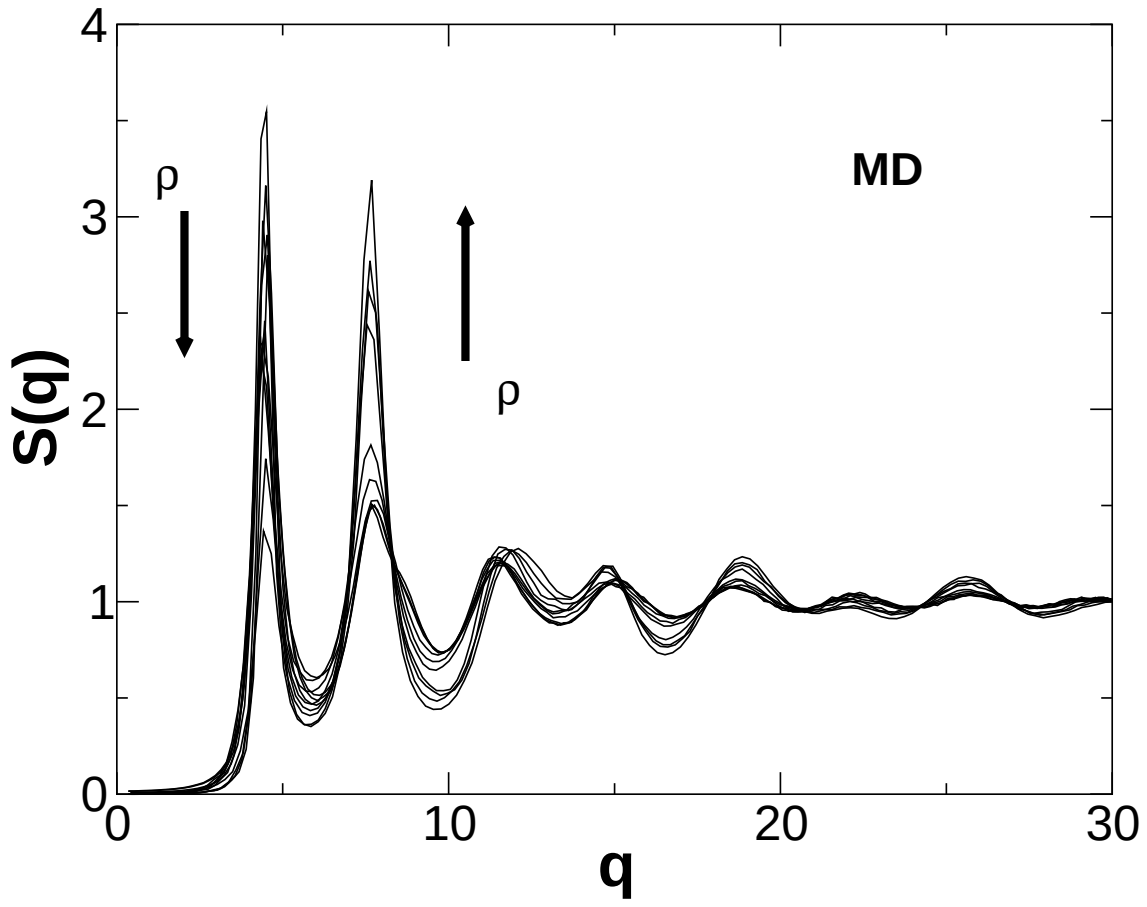

FIG. 3: Density dependence of the structure factor at $T = 0.063$. Note the progressive reduction of the amplitude of the first peak and the progressive increase of the second peak on increasing ρ. Different curves refer to $\rho = 0.272$, 0.296, 0.322, 0.352, 0.384, 0.421, 0.464, 0.512, 0.567, 0.629, and 0.702.

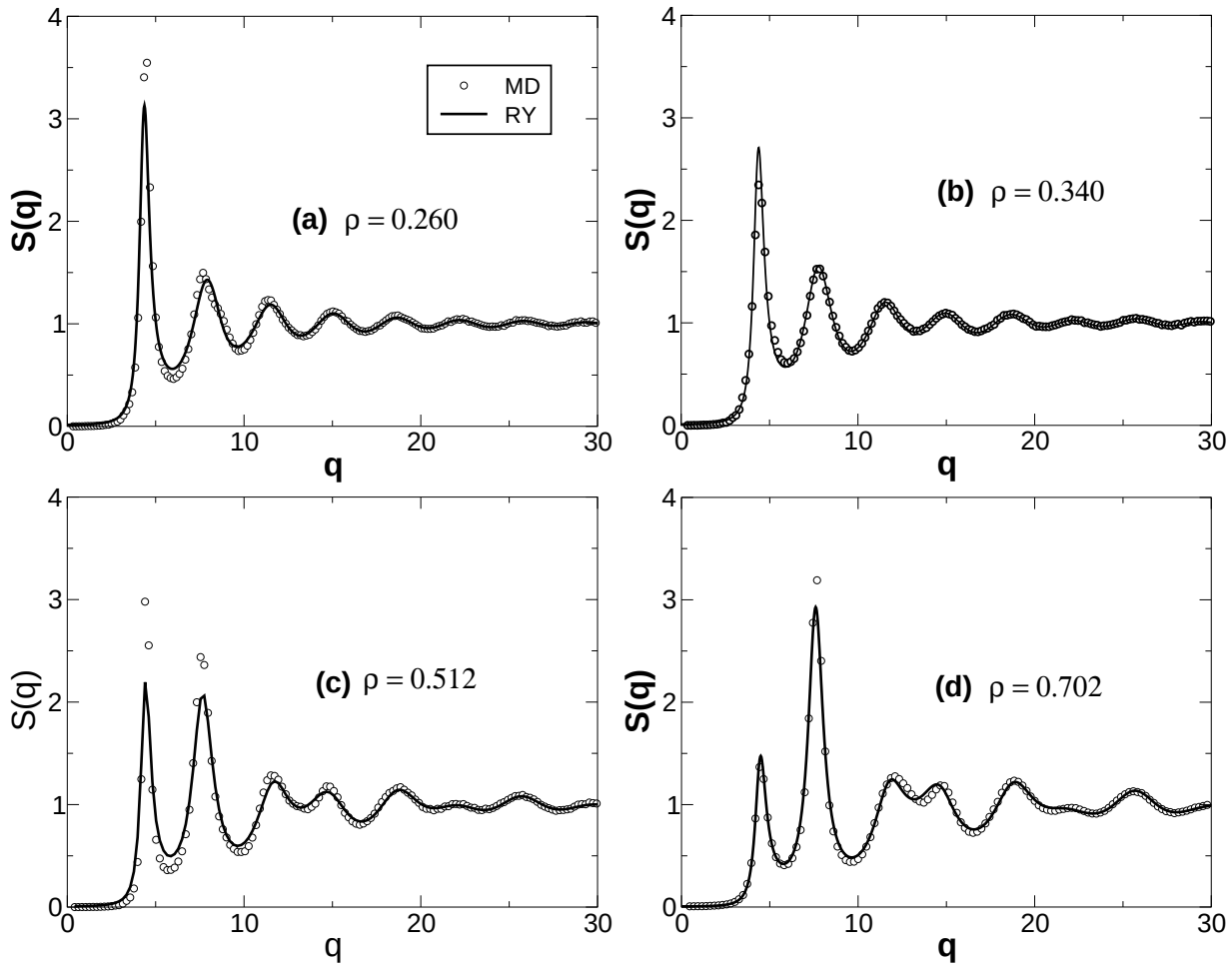

FIG. 4: Comparison of the static structure factor, obtained in simulations and in the RY closure for (a) low density $\rho = 0.260$, (b)–(c) intermediate densities $\rho = 0.340$ and $\rho = 0.502$, and (d) high density $\rho = 0.702$.

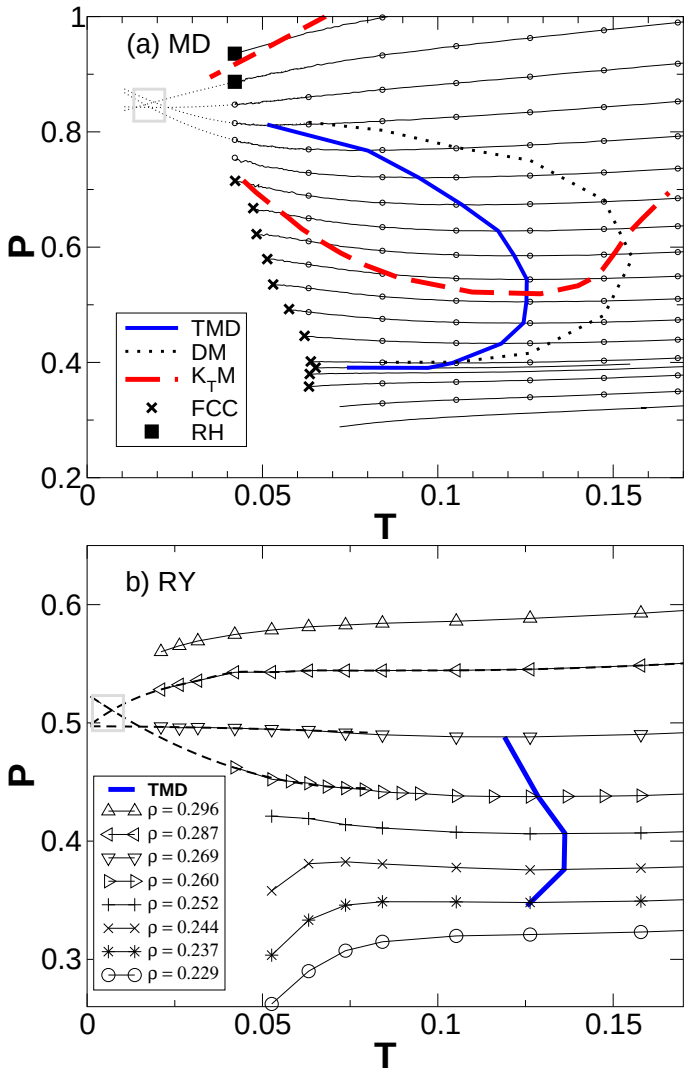

FIG. 5: (a) Phase diagram of a system of particles interacting via the potential defined in Eq. (2) with $n = 144$. Lines indicate $P(T)$ for several isochores at the following values of ρ, from top to bottom: 0.378, 0.364, 0.352, 0.340, 0.328, 0.317, 0.306, 0.296, 0.287, 0.277, 0.269, 0.260, 0.252, 0.244, 0.242, 0.240, 0.237, 0.229, 0.223. Also shown are the locus of density maxima ($\partial V/\partial T|_P = 0$) (bold blue line), the locus of compressibility maxima and minima $\partial V/\partial P|_T = 0$ (dashed red line), and the locus $\partial D/\partial P|_T = 0$ (bold dotted line). At low ρ, lines terminate when the system crystallizes or does not equilibrate within the available simulation time. Note that different crystals, fcc and rhombohedral, are found for $\rho < 0.317$ and $\rho > 0.352$, respectively. The extrapolated isochores at large ρ cross at a finite T (open box), consistent with the possibility of a liquid-liquid critical point for T below the ones that can be investigated numerically. (b) Corresponding phase diagram obtained within the RY closure. An extrapolation of the isochores also shows the possibility of a very low temperature liquid-liquid phase transition.

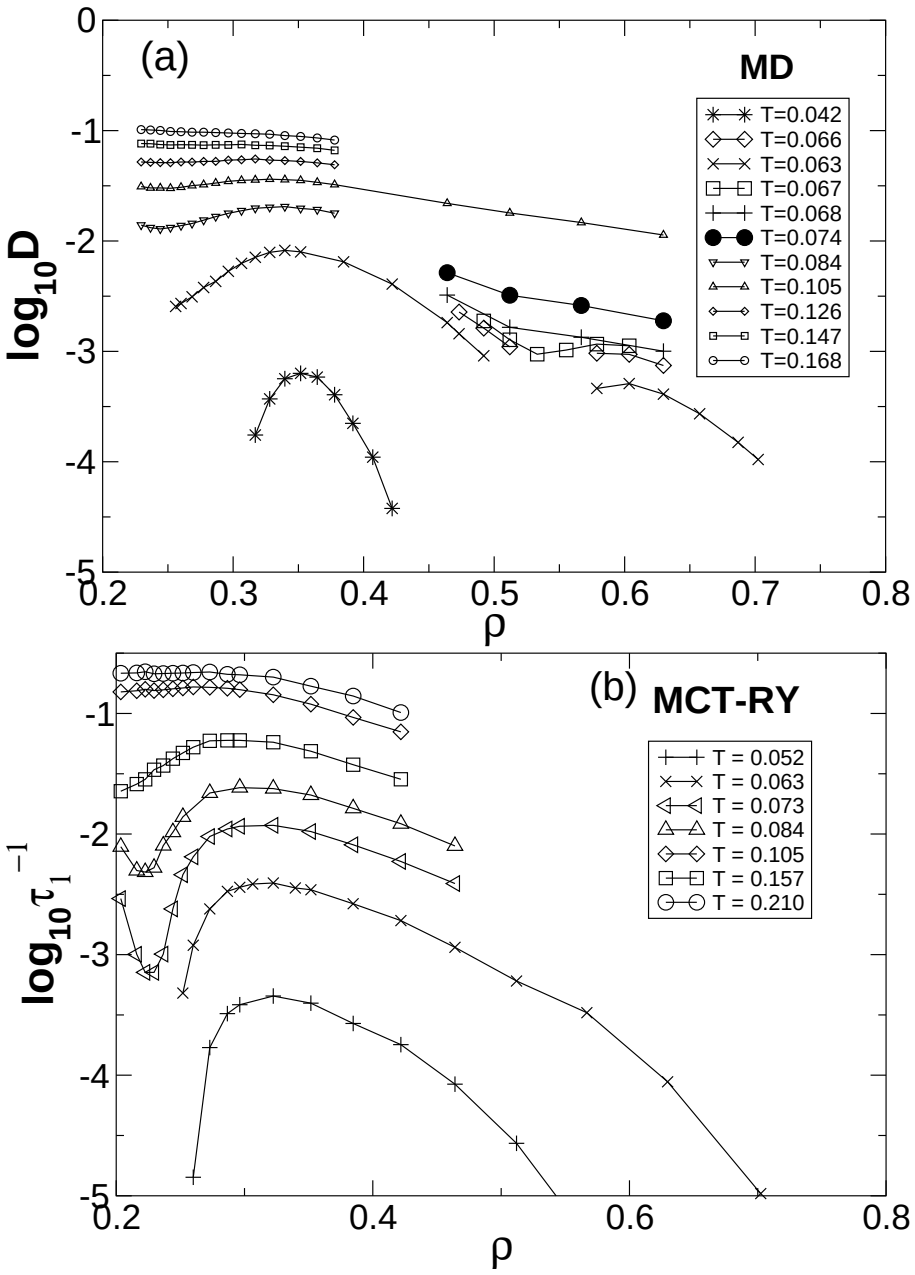

FIG. 6: (a) The behavior of the diffusion coefficient as a function of density ρ for several isotherms obtained from MD simulations. (b) The density autocorrelation time τ_1^{-1} from MCT-RY. At low temperatures when the density is very high or low, τ_1 increases sharply, showing the transition to a glassy state. Note the similar behavior of D and τ_1^{-1}.

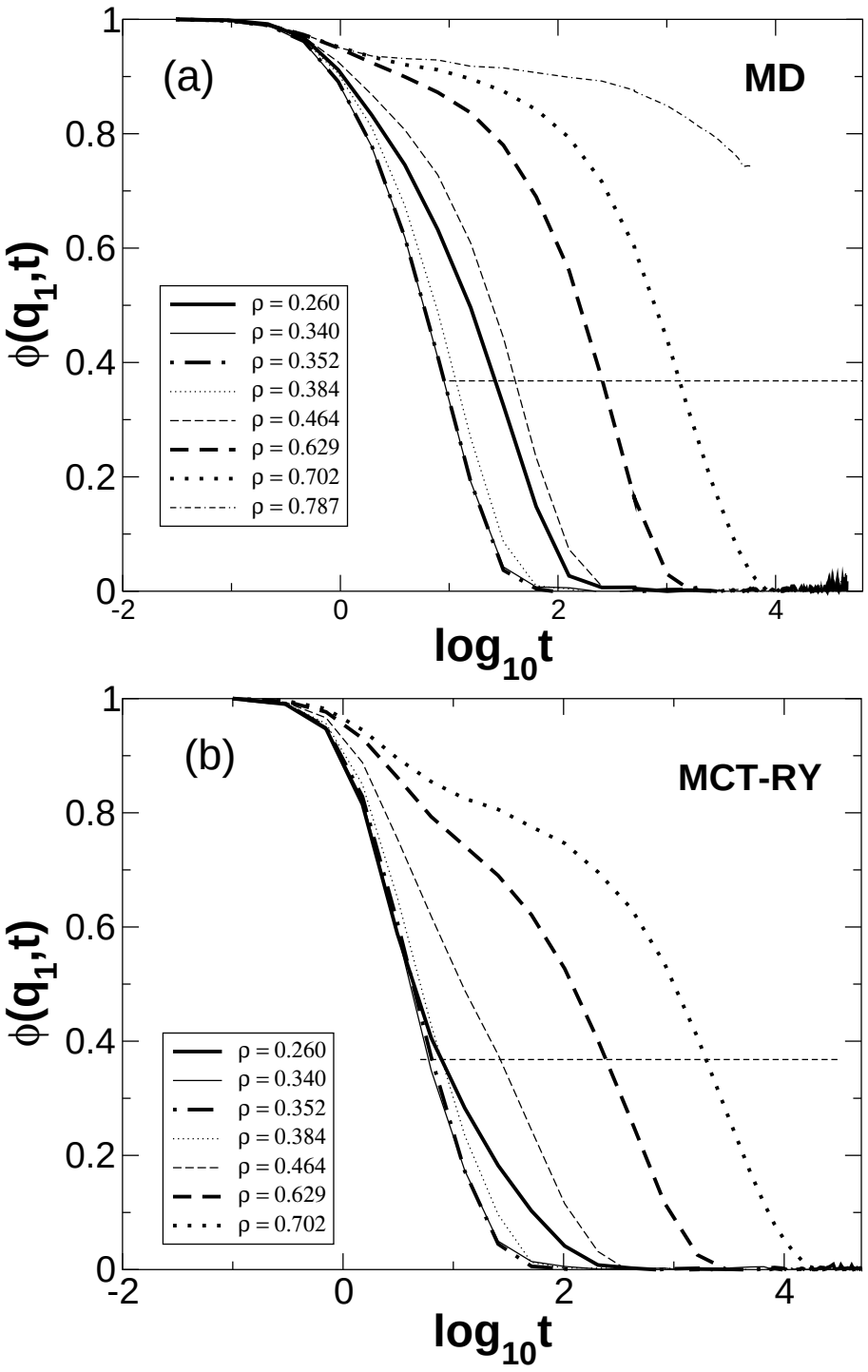

FIG. 7: The behavior of the correlators for the wave vector q_1 corresponding to the first peak of the static structure factor for $T = 0.063$ for (a) MD and (b) MCT-RY. The dashed horizontal line indicates the $1/e$ value used to define the characteristic time τ_1.

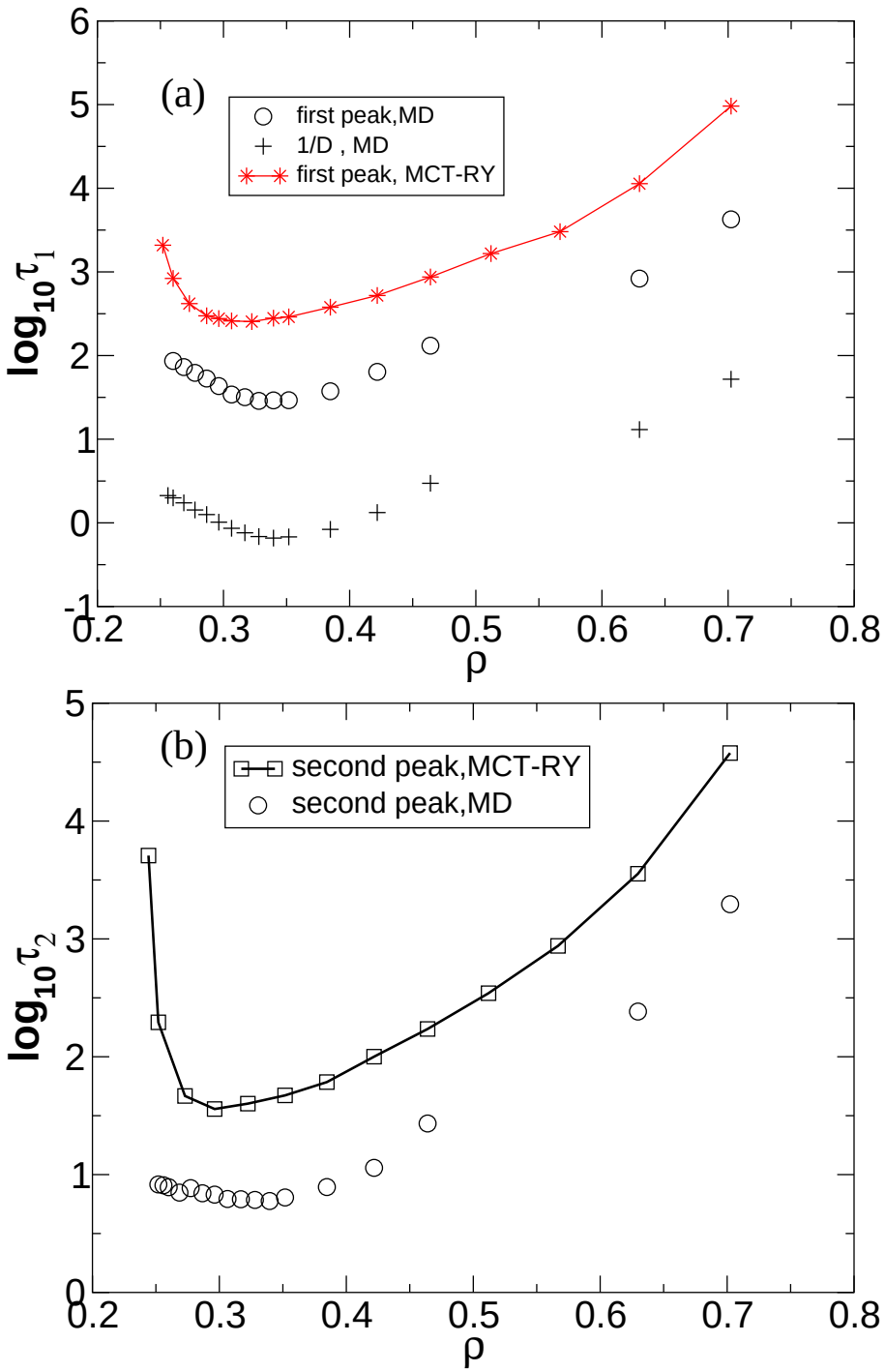

FIG. 8: The density behavior of the correlation times (a) τ_1, and (b) τ_2, obtained directly from MD simulations for $T = 0.063$ and for the MCT calculations based on RY. The behavior of the diffusion coefficient is also shown. All curves show the anomalous decrease with density for small densities.

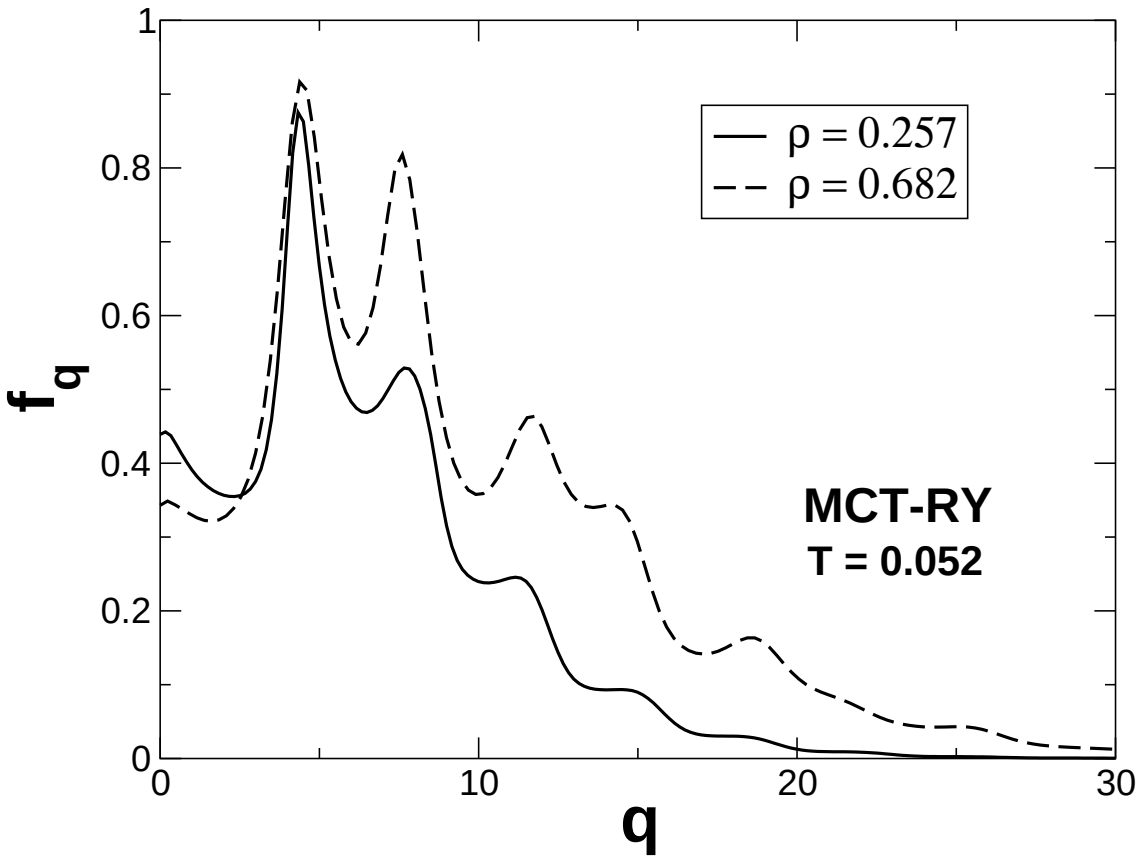

FIG. 9: The behavior for $T = 0.052$ of the critical non-ergodicity parameter f_q for the two critical densities $\rho = 0.257$ and $\rho = 0.682$.

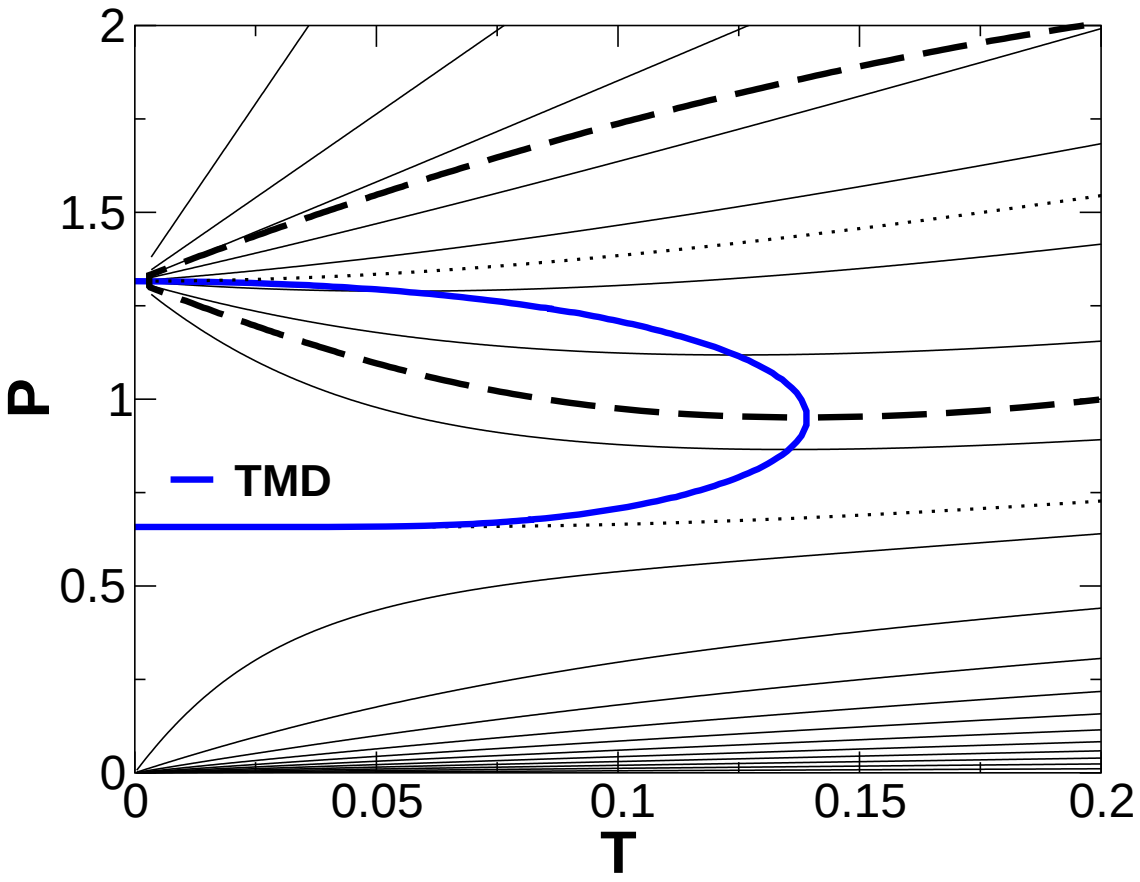

FIG. 10: The $P-T$ phase diagram of the one-dimensional system with the ramp potential ($\sigma_0 = 1, \sigma_1 = 1.76, U_0 = 1$) defined in Eq. (1). The thin solid lines are isochores for $\rho = 0.05, 0.1, ..., 0.95$ from bottom to top. The bold dotted lines are isochores for $\rho = 1/\sigma_1$ and $\rho = 2/(\sigma_0 + \sigma_1)$ between which the density anomaly region bounded by the temperature of the maximal density line (bold blue line) is located. The dashed bold line bounds the region of anomalous isothermal compressibility extrema (both minima and maxima).